UNIVERSITY OF MINNESOTA

ST. ANTHONY FALLS HYDRAULIC LABORATORY

LORENZ G. STRAUB, DIRECTOR

Technical Paper No. 41, Series B

TURBULENT BOUNDARY LAYER FLOW OVER A FLAT PLATE VIBRATING WITH TRANSVERSE STANDING WAVES

by

Albert G. Mercer

Prepared for
David Taylor Model Basin

Department of the Navy
Washington, D.C.
under
Bureau of Ships Fundamental Hydromechanics Research Program
SR-009-01-01
Office of Naval Research Contract Nonr 710(38)

September, 1962
Minneapolis, Minnesota

CER62AGM88

UNIVERSITY OF MINNESOTA
ST. ANTHONY FALLS HYDRAULIC LABORATORY
LORENZ G. STRAUB, Director

Technical Paper No. 41, Series B

Turbulent Boundary Layer Flow over a Flat Plate Vibrating with Transverse Standing Waves

by

ALBERT G. MERCER

Prepared for
DAVID TAYLOR MODEL BASIN
Department of the Navy
Washington, D. C.
under
Bureau of Ships Fundamental Hydromechanics Research Program
SR-009-01-01
Office of Naval Research Contract Nonr 710(38)

September, 1962
Minneapolis, Minnesota

A B S T R A C T

An attempt is made to show theoretically that the drag caused by a turbulent boundary layer on a smooth flat plate vibrating with low amplitude transverse standing waves is the same as for a non-vibrating plate provided the wave celerity of the component traveling waves is greater than about 3.5 times the free stream velocity. Experiments conducted in a water tunnel with a rectangular cross-section having one vibrating wall showed no measurable change in boundary layer velocities, as compared to non-vibrating conditions, for frequencies ranging from 15 to 122 cps and free stream velocities ranging from 2.4 to 15 fps. The lowest wave celerity to free stream velocity ratio tested was 2.54.

CONTENTS

LIST OF ILLUSTRATIONS

LIST OF SYMBOLS

a - wave amplitude, 1/2 crest to trough height

c - wave celerity

c_f - drag coefficient for the undisturbed flow

c_f' - local drag coefficient for the undisturbed flow

c_w - drag coefficient caused by the presence of a wave; based on surface area

d - thickness of the vibrating plate

D - Tietjens function

E - Young's modulus of elasticity

f - wave frequency

F - a residue function related to the perturbation velocity

F_i - inertial force due to the mass of the vibrating plate

J - Jacobian of the transformation to curvilinear co-ordinates

k - equivalent to $\frac{2\pi}{\lambda}$

m - a parameter used in the Tietjens function

p_o - wall pressure

P_o - peak wall pressure. P_{o_i} and P_{o_r} are the real and imaginary components.

R - Reynolds number of the flow based on the distance from the leading edge.

s - sheltering coefficient

S - specific gravity of the plate material

u - velocity component in the ξ or x direction, depending on co-ordinate systems

U - boundary layer velocity without waves

v - velocity component in the η or y direction, depending on co-ordinate systems

V_o^* - the wall shear velocity of the undisturbed flow

z - the variable of Tietjens function; z_o is the boundary value

γ - specific weight of water

η - curvilinear co-ordinate in the direction across the flow

ϕ_1 - inviscid component of the function F

ϕ_2 - viscous component of the function F

λ - wave length--spans two loops for standing waves

ν - kinematic viscosity

ξ - curvilinear co-ordinate in the direction parallel to the flow

ρ - mass density of the fluid

τ_o - wall shear

ψ - stream function for flow with boundary waves

ψ_o - stream function for flow without boundary waves

ψ_p - stream function perturbation due to boundary waves

TURBULENT BOUNDARY LAYER FLOW OVER A FLAT PLATE VIBRATING WITH TRANSVERSE STANDING WAVES

I. INTRODUCTION

Fluid drag on a flat plate in steady motion is fairly easy to estimate. Recently, increased attention has been given to flow past wavy boundaries. This interest was first directed to the problem of the generation of surface waves by wind. Benjamin [1]* summarizes the work of previous researchers in this field, notably that of Miles [2].

It is generally established that drag is imposed on the flow by the wave by a sheltering effect wherein the pressure on the windward side of the wave is higher than on the leeward side. This effect can be explained conveniently by the phenomenon of separation. Miles, however, by taking viscosity into account, showed that sheltering can occur without separation. Benjamin in his paper generalizes the work of Miles and computes a sheltering effect for a laminar boundary layer profile. He proposes that the method is extendable, with limitations, to turbulent boundary layer profiles. He reports agreement with the work of Motzfeld [3] who experimentally discovered a sheltering pressure distribution without separation for flow over fixed waves with steepnesses of 0.025.

More recently, tests by Kramer [4] indicated that stabilization of laminar boundary layers could be accomplished by applying to the surface a compliant dissipative coating in which traveling waves are generated by the flow. A discussion and analysis of this phenomenon is also given by Benjamin [5]. In the above situations it is important to realize that the wave celerity c is always less than the main stream flow velocity.

Another problem of waves on boundary surfaces involves the plates of ship hulls. Vibrations within the ship cause standing waves to be excited in the plates. The objective of the research on which this report is based was to determine if these standing waves influence the boundary layer to the extent of causing an additional drag. Tests were conducted in a horizontal water tunnel having a rectangular cross-section 8 in. deep and 12 in. wide. A flexible steel plate 12 in. wide and 45 in. long composed part of the upper

---

*Numbers in square brackets refer to the List of References on p. 27.

surface. This plate was vibrated with frequencies ranging from 15 to 122 cps. Velocity traverses upstream and downstream of the vibrating section were made for several frequencies within this range and for core velocities ranging from 2.4 to 15 fps. In these tests the boundary layer appeared completely unaffected by the state of vibration. Analysis based on the work by Benjamin [1] on traveling waves has been adapted to standing waves by superposition to confirm this result.

This research was carried out under the Bureau of Ships Fundamental Hydromechanics Research program, SR-009-01-01, administered by the David Taylor Model Basin. Grateful acknowledgment is expressed to the members of the Laboratory staff who participated in this program. Particular acknowledgment is expressed to K. Yalamanchili who aided in the preliminary stages of the project, to Z. S. Tarapore who collected much of the data, and to Carol Takyi who prepared the manuscript under the direction of Loyal Johnson. This study has been conducted under the general direction of Dr. Lorenz G. Straub, Director of the Laboratory.

II. THEORETICAL DESCRIPTION OF THE FLOW

A. General Theory for Traveling Waves

In his paper, Benjamin [1] analyzed the action of shearing flows passing over a boundary surface disturbed by a continuous train of harmonic waves. The waves travel along the flexible but stationary surface with a celerity c. His analysis parallels that used in the study of the stability of laminar boundary layers. In the stability study a simplification of the Navier-Stokes equation, known as the Orr-Summerfeld equation, is used to analyze the behavior of small amplitude traveling wave disturbances assumed to exist within the boundary layer flow. The relationship between wave celerity, wave length, and amplitude attenuation is determined for different Reynolds numbers. Conditions favoring a negative attenuation are assumed to be unstable.

The Orr-Summerfeld equation also arises in this analysis of flow over a traveling surface disturbance. However, in this case the wave length, amplitude, and celerity are given a priori as a property of the boundary. The character of the disturbance to the flow caused by the wave is determined to find out if the wall stresses are such as to cause an extra drag on the surface. The extra drag is caused by a sheltering effect in which the pressure

distribution is out of phase with the wave form so that the pressures on the downstream side of the wave are less than those on the upstream side. This is not to be confused with the amplifying effect caused by pressure distributions in phase with the wave that is important in stability studies. The salient points of the analysis are presented in the remaining paragraphs of this subsection.

Two transformations are introduced at the beginning of the analysis to bring the boundary conditions into a more tractable form. First, to achieve a steady flow situation the co-ordinate system is referenced to the wave celerity. The wave form is thereby fixed in space but the surface itself and the flow are given an additional velocity component -c. Second, curvilinear orthogonal co-ordinates are used, corresponding to the stream function and the potential function for potential flow over the wavy surface. The co-ordinate η is directed across the flow and the co-ordinate ξ is directed along the flow. The ξ,η system is correlated to a rectangular x, y system by the complex transformation.

$$\xi + i\eta = x + iy - iae^{ik(x + iy)}, \quad k = \frac{2\pi}{\lambda} \tag{1}$$

where λ is the wave length and a is the wave amplitude. The equation for the boundary surface is simply $\eta = 0$. With the flow transformed onto the ξ, η plane the boundary is a flat surface.

The stream function for the disturbed flow $\psi(\xi,\eta)$ is assumed to have two components. The first $\psi_o(\eta)$ is the stream function for the main shear flow assuming no wave, i.e. $\eta = y$. It is given by

$$\psi_o = \int_0^{\eta} [U(\eta) - c]\, d\eta \tag{2}$$

where $U(\eta)$ is the undisturbed velocity. The second component $\psi_p(\xi,\eta)$ is the periodic harmonic perturbation caused by the wave and is written for later convenience in the form

$$\psi_p = [F(\eta) + (U(\eta) - c)e^{-k\eta}]\, ae^{ik\xi} \tag{3}$$

where $F(\eta)$ is a residue function to be computed. The complex notation takes into account a possible phase shift in reference to the wave form. The

remaining analysis requires that the wave steepness be small so that the terms k^2 and ak are of second order magnitude.

The velocity of the disturbed flow to first order in ak can be described by components in the ξ and η directions using the respective equations.

$$\begin{aligned} u(\xi,\eta) &= J^{\frac{1}{2}}\psi_\eta = U - c + a[F' + U'e^{-k\eta}]\,e^{ik\xi} \\ v(\xi,\eta) &= -J^{\frac{1}{2}}\psi_\xi = -ika[F + (U - c)e^{-k\eta}]\,e^{ik\xi} \end{aligned} \tag{4}$$

where J is the Jacobian of the co-ordinate transformation. Here again the complex notation allows for a phase shift even though only the real parts of u and v are to have meaning.

The two-dimensional Navier-Stokes equations for laminar flow, when written in terms of the stream function, yield upon elimination of the pressure terms the following expression for F.

$$(U - c)(F'' - k^2F) - U''F = -i\,\frac{\nu}{k}\,[F^{iv} - 2k^2F^2 + k^4F]e^{-k\eta} \tag{5}$$

assuming parallel main flow (U''' and $U^{iv} = 0$). This is the Orr-Summerfeld equation which is basic to the theory of boundary layer stability. (See Schlicting [6], page 316.) For reasonably high Reynolds numbers, the viscous terms on the right are small and negligible except in special friction layers. One of these occurs at the boundary and another occurs in the region, if any, where $U(\eta)$ approaches c. In our problem, c will be shown to be larger than U for all practical cases so that this second layer will not exist.

The function $F(\eta)$ can be resolved handily into two components which are additive. The first $\phi_1(\eta)$ is an inviscid function which satisfies (5) when the right hand terms are neglected to give

$$(U - c)(\phi_1'' - k^2\phi_1) = U''\phi_1 \tag{6}$$

The second $\phi_2(\eta)$ is a viscous function which is negligible everywhere except near the boundary and which satisfies the equation

$$(U - c)\phi_2'' = -i\,\frac{\nu}{k}\,\phi_2^{iv} \tag{7}$$

This equation is obtained from Eq. (5) by neglecting the terms containing U'' and k^2. The terms containing these values are small at the boundary.

Both ϕ_1 and ϕ_2 must approach zero as $\eta \to \infty$. The other boundary conditions are

$$\phi_1(o) + \phi_2(o) = c \quad \text{and} \quad \phi_1'(o) + \phi_2'(o) = -U'(o) \tag{8}$$

Solutions of ϕ_1 and ϕ_2 that approach zero at infinity will each contain one undetermined coefficient. The coefficient for ϕ_1 can be obtained from the combined boundary condition

$$\phi_1'(o) - \frac{\phi_2'(o)}{\phi_2(o)}\,\phi_1(o) = -U'(o) - c\,\frac{\phi_2'(o)}{\phi_2(o)} \tag{9}$$

The coefficient for ϕ_2 follows from ϕ_1, and Eq. (8).

The pressure on the boundary as related to the pressure at infinity can be obtained by integrating the simplified Navier-Stokes equation along a ξ line from $\eta = 0$ to $\eta = \infty$. The function ϕ_1 is significantly large for η up to about $\frac{\lambda}{2}$ but the region of significant ϕ_2 is very small. The function ϕ_2 is therefore negligible in this integration and the pressure can be expressed by

$$p_o - p_\infty = P_o e^{ik\xi}, \quad P_o = \rho a k^2 \int_0^\infty (U - c)\phi_1 \, d\eta \tag{10}$$

Shear due to the wave action, on the other hand, is almost entirely attributable to ϕ_2 and is given by

$$\tau_o = \mu \phi_2''(o) a e^{ik\xi} \tag{11}$$

p_o and τ_o are seen to be harmonic with respect to ξ but possibly out of phase with the wave form.

The extra drag induced by the wave action is computable from these boundary stresses. First from Eq. (10) it follows that the real and imaginary components of ϕ_1 will give respectively real and imaginary components of P_o. The real component P_{o_r} will give a negative pressure distribution

phased with the wave form. This distribution will contribute zero net form drag. The imaginary component P_{o_i} gives a pressure distribution $\frac{\lambda}{4}$ out of phase with the wave and a net drag does result. This is the so-called sheltering effect.

The resulting drag coefficient is given by the expression

$$c_w = \frac{\pi}{2} \frac{akP_{o_i}}{\rho U_\infty^2} \tag{12}$$

The harmonic shear distribution, of course, contributes no net drag.

The function ϕ_1 would ordinarily be real since Eq. (6) has only real parts. However, the function ϕ_2 is complex and through the combined boundary conditions of Eq. (9) a complex character can be transferred to ϕ_1. Therefore, although ϕ_1 is essentially inviscid in origin, its final form is influenced by the viscid function ϕ_2. The effect of ϕ_2 on ϕ_1 is as though a "displacement thickness" were created along the boundary. The thickness varies harmonically, but out of phase, with the wave form producing a falsely-shaped boundary for the inviscid flow.

An effect more important in boundary layer stability and wave generation is the complex character that ϕ_1 receives due to the singularity of the point where $U = c$. As mentioned before, however, this situation is not important to this paper.

B. A Traveling Harmonic Wave with No Main Flow

The simplest model to which this theory can apply is the one in which there is no main shear flow. This case is not treated by Benjamin [1]. However, investigation of this problem will bring out the character of the analysis, especially as it applies to the present study. $U(\eta)$ now is identically zero and Eqs. (6), (7), and (8) have the exact solutions

$$\phi_2(\eta) = -(i + 1)\nu \sqrt{\frac{kc}{2\nu}} \exp\left(\sqrt{\frac{kc}{2\nu}} (i - 1)\eta\right) \tag{13}$$

and

$$\phi_1(\eta) = c\left[1 + (i + 1)\frac{\nu}{c}\sqrt{\frac{kc}{2\nu}}\right] \exp\left[-k\eta\left(\frac{1 - (i - 1)\frac{\nu}{c}\sqrt{\frac{kc}{2\nu}}}{1 + \frac{2\nu}{c}\sqrt{\frac{kc}{2\nu}}}\right)\right] \tag{14}$$

The expression for ϕ_1 is complicated, but if the variable $k\nu/c$ is small Eq. (14) reduces to

$$\phi_1(\eta) = ce^{-k\eta} \tag{15}$$

Since both k and ν are small, this equation must hold except for the very slowest wave celerities ($c < 1$). The velocities associated with ϕ_1, obtainable from Eq. (4), are

$$\begin{aligned} u(\xi,\eta) &= -akce^{-k\eta} \cos k(\xi - ct) \\ v(\xi,\eta) &= +akce^{-k\eta} \sin k(\xi - ct) \end{aligned} \tag{16}$$

In these equations the wave form celerity has been restored. This is exactly the potential flow under a moving wave. The wall pressure distribution from Eq. (10) has the form

$$P_o - p_\infty = -\rho(kc)^2 \frac{a}{k} \cos k(\xi - ct) \tag{17}$$

Figure 1 shows the potential flow for this problem and the resulting velocities and stress distributions. The depth at which the potential velocity is 1 per cent of the boundary velocity is 0.73λ.

The viscid solution $\phi_2(\eta)$ is also recognizable. It is equivalent to the boundary layer on a flat oscillating plate (see Schlicting [6], page 67). The u component of velocity becomes

$$u(\xi,\eta) = akc \exp\left(-\sqrt{\frac{kc}{2\nu}}\eta\right) \cos\left(\sqrt{\frac{kc}{2\nu}}\eta + k(\xi - ct)\right) \tag{18}$$

The wall shear due to the viscid solution is given by

$$\tau_o = -\mu a(kc)\sqrt{\frac{kc}{\nu}} \sin\left(k\xi + \frac{\pi}{4} - kct\right) \tag{19}$$

The velocity pattern and shear for this function are shown as well in Fig. 1. The thickness over which the viscid solution is significant has been called the wall friction layer. Its thickness may be estimated by the magnitude of the quantity $\sqrt{2\nu/kc}$ which is for most conditions very small.

The above analysis shows that the flow pattern beyond the wall friction layer is very accurately represented by the usual potential flow except for cases where $k\nu/c$ approaches 1 or larger. This usually requires very low wave celerities. The viscosity is shown to be directly influential only in a very narrow friction layer next to the boundary.

The possibility of a sheltering effect due to a zone of separation in the lee of the wave form is definitely not present in this case. A fluid-filled cavity following the wave would have to be transported over the stationary boundary at a velocity c. This situation is, obviously, impossible.

C. A Standing Harmonic Wave with No Main Flow

The second model worthy of consideration is the case of a standing harmonic wave as shown in Fig. 2. A standing wave with amplitude a, wave length λ, and frequency f can be produced by the superposition of two traveling wave trains with equal and opposite celerities. These waves must each have an amplitude of $\frac{1}{2}a$, a wave length of λ and celerities c equal to plus and minus λf. It is useful to note here that $kc = 2\pi f$. The flow pattern for a standing wave can be obtained by the corresponding superposition of the traveling wave flow patterns. This is entirely acceptable within the limitations of small wave steepnesses and the neglect of second order terms.

Figure 2 shows the result of superimposing the flow patterns. When the plate is in the null position the potential streamlines and velocity patterns are exactly the same as for traveling waves. In the loop position the inviscid velocities are everywhere zero. It is interesting to note that the viscous velocities reinforce at the nodes but cancel at the loops. Although it is not shown in the figure, the viscous velocities do not all become zero when the plate is in the loop position due to a time phase shift.

The pressure distribution has a standing wave pattern in phase timewise and anti-phase spacewise with the wave form. In the case of the traveling wave, a sheltering effect could only be achieved if the quantity $k\nu/c$ approached 1. In the present case the sheltering effect, if any, is automatically cancelled out. This result would be suggested also by the symmetry of the flow pattern.

There is, of course, no separation possible in this case either. The particles near the boundary are confined to small orbital paths and do not accumulate in a zone of separation.

D. A Traveling Wave with a Turbulent Boundary Layer

Turbulent boundary layers would seem to be applicable to the general theory as long as the friction layer lies within the laminar sublayer, or at least not too far beyond it.

Most of the analysis in the preceding paragraphs comes from Benjamin [1]. For the case of boundary layer flow solutions of Eqs. (6), (7), and (8) are not obtained exactly. Simplification of Eq. (7) can be accomplished by assuming the velocity of the boundary layer U to be linear as in the laminar sublayer, so that $U = \eta U'(o)$. All the coefficients in Eq. (7) are thereby constant with η. Equation (7) in this new form has been solved numerically in connection with boundary layer stability studies. Tabular values of the function ϕ_2 are presented for instance in Holstein [7]. The variable η, however, is replaced by a new variable, z, defined by

$$z = m\eta - \frac{mc}{U'(o)}, \quad \text{where} \quad m = \left(\frac{cU'(o)}{\nu} \right) \tag{20}$$

Notice that on the boundary $z_o = -mc/U'(o)$. The function ϕ_2 decreases very rapidly with increasing z or η so that the wall friction layer is again very thin. It is found to be negligible by the time η reaches $1/m$.

Of special value in Eq. (9) is the Tietjens function $D(-z_o)$ defined by

$$D(-z_o) = -m \frac{\phi_2(o)}{\phi_2'(o)} \tag{21}$$

The real and imaginary parts of D are tabulated in Holstein [7], and graphed in Benjamin [1]. Both components of D approach zero as $-z_o$ becomes fairly large. In any event, it is $O(1)$ or less for practical values of $-z_o$.

A simple approximate inviscid solution to Eq. (6) is

$$\phi_1 = +B(c - U)e^{-k\eta} \tag{22}$$

It holds fairly well as long as no singularity occurs as, for instance, where U = c. The coefficient B comes from consideration of Eq. (9) and has the form

$$B = \frac{1 + D(-z_o)/z_o}{1 + D(-z_o)/z_o + D(-z_o)/m} \tag{23}$$

If the term $-z_o$ is $O(D(-z_o))$, D in Eq. (23) will dominate and ϕ_1 will be complex, giving rise to a sheltering effect. However, if $-z_o$ is much larger than D, B will approach the real value 1, ϕ_1 will be real, and there will be no sheltering effect. Inspection of the function D shows that for $-z_o > 8$, $|D(-z_o)|$ is less than 0.25 and decreases to approach zero as $-z_o$ increases. Therefore for $-z_o > 8$ sheltering would be negligible.

It is a relatively simple matter to show that $-z_o > 8$ is met providing $c > 5U_\infty$. From the study of turbulent boundary layers (see Schlicting [6], page 432.) the velocity gradient at the wall can be related to the core velocity by the equation

$$U'(o) = c_f' U_\infty^2 / 2\nu \tag{24}$$

where c_f' is the local drag coefficient dependent on the Reynolds number. Introducing Eq. (24) into the expression defining z_o and eliminating m gives the relationship

$$\frac{c}{U_\infty} = \left[\frac{(-z_o)^3}{4\nu}\right]^{\frac{1}{4}} \sqrt{c_f'} \tag{25}$$

According to Schlicting, for Reynolds number greater than 10^5 the quantity c_f' is less than 0.0055. Substitution of $-z_o = 8$, $\nu = 10^{-5}$, and $c_f' = 0.0055$ into Eq. (24) gives $c = 4.4U_\infty$. It follows therefore that for turbulent boundary layers the general theory indicates a negligible sheltering effect provided the wave celerity is greater than about five times the main stream velocity.

It remains to determine a criterion which insures that the general theory itself is applicable to a particular situation. The restriction is

that the wall friction layer, which extends to about $\eta = \frac{1}{m}$, should lie within the region of linear velocity. According to Benjamin this region extends to $\eta = 10\nu/V_o^*$ even though the usual expression for the extent of the laminar sublayer is $\eta = 5\nu/V_o^*$. Equating the expressions for these two regions and introducing again Eq. (24) gives the expression

$$\frac{c}{U_\infty} = \frac{\sqrt{c_f'}}{4000\nu} \tag{26}$$

Substituting $\nu = 10^{-5}$ and $c_f' = 0.0055$ produces the result that $c = 5.2U_\infty$.

A wave celerity greater than five times the main stream velocity would seem to be an adequate criterion to insure that there be no sheltering due to the effects of the wall friction layer. Apparently the wave length and wave amplitude are not directly significant. The effect of the boundary layer thickness is reflected in the effect of Reynolds number on c_f'. For $R > 10^9$, c_f' is less than 0.0014 and the criterion becomes c greater than $2.6U_\infty$.

Sheltering caused by a zone of separation following the wave form is also impossible under the above criterion. The reasoning is the same as given in the case of a traveling wave with no flow. A convenient point of view from which to observe this situation is with the reference velocity adjusted so that the wave form is stopped. With this reference it can be seen that there is no area of flow reversal as long as c is greater than U_∞.

The only remaining mechanism by which the traveling wave could influence the main flow is interference in the turbulence pattern. This possibility is completely unlikely as long as the wall friction layer lies within the laminar sublayer as required by the above criterion. The oscillating movements of the potential flow alone produce no strong shears that could influence the turbulence.

The equation for the wall pressure distribution for a turbulent boundary layer may be obtained by substituting Eq. (22) for ϕ_1 with $B = 1$ into Eq. (10) for p_o to get

$$p_o - p_\infty = -\rho k^2 a e^{ik\xi} \int_0^\infty (1 - \frac{U(\eta)}{c})^2 c^2 e^{-k\eta} d\eta \qquad (27)$$

U_∞ can be substituted for $U(\eta)$ without materially affecting the results, especially if c is large. Upon integration of Eq. (27) and restoration of the wave velocity the expression for pressure is

$$p_o - p_\infty = - (1 - \frac{U_\infty}{c})^2 \rho(kc)^2 \frac{a}{k} \cos k(\xi - ct) \qquad (28)$$

which is comparable to Eq. (17) for the case of no flow.

E. A Standing Wave with a Turbulent Boundary Layer

The research of this report involved a case of turbulent boundary layer over a boundary surface vibrating with standing waves. A criterion for the existence of a sheltering effect for this case can be obtained by superimposing the appropriate turbulent boundary layer traveling wave situations. It is first necessary, however, to reconsider the previous case of traveling waves with a turbulent boundary layer but with the flow velocity and the wave celerity opposite in direction to each other. The variable z must be redefined compared with Eq. (20) to give

$$z = -m\eta - \frac{mc}{U'(o)} \qquad (29)$$

where the definition of m is unchanged. Since m and $U'(o)$ in this case are numerically negative, the relationship between z and $\phi_2(z)$ and η is exactly as before. In order to make use of existing tables and graphs, the Tietjens function should be redefined as

$$D(-z_o) = + m\phi_2(o)/\phi_2'(o) \qquad (30)$$

When these adjustments are made, the criterion previously established can be applied equally well to this reversed case.

For analysis, the turbulent boundary layer passing over a standing wave must be separated into two equivalent boundary layers, each moving over

oppositely directed traveling waves. These equivalent boundary layers will each contain half the undisturbed main flow so that all velocities are half of the undivided flow velocities. The important distances from the wall such as the thickness of the boundary layer and the thickness of the laminar sublayer are unchanged by this arbitrary division. The wall velocity gradient will be $\frac{1}{2}U'(o)$ where the symbol refers to the undivided flow. A boundary layer with a free stream velocity equal to $\frac{1}{2}U_\infty$, developing naturally, would, however, have quite different proportions. The thickness of the laminar sublayer would be roughly twice that of the undivided flow and the wall velocity gradient would be only roughly $\frac{1}{4}U'(o)$. The naturally developing boundary layer is unimportant to this analysis, however, since the criterion to be developed depends only on the character of ϕ_2 which in turn depends only on the conditions at the boundary and not on the method of development.

To find a relationship between c and U_∞ for the undivided flow, it is only necessary to refer to Eqs. (25) and (26). In Eq. (25) c must be adjusted so that $-z_o$ remains constant at 8. Therefore c must vary as the root of c_f'. This relationship holds for Eq. (26) as well. Substituting $\frac{1}{2}U'(o)$ and $\frac{1}{2}U_\infty$ into Eq. (24) shows that the local drag coefficient for the divided flow is $2c_f'$. Substituting $2c_f'$ and $\frac{1}{2}U_\infty$ into Eq. (25) or Eq. (26) shows that c must be $\sqrt{2}\,5U_\infty$ or about $3.5U_\infty$. Therefore for Reynolds numbers based on distance from the leading edge greater than about 10^5 there is negligible sheltering due to the wave disturbance provided c is greater than $3.5U_\infty$. For R greater than 10^9 the lower values of c_f' require that c need only be greater than $2U_\infty$.

Separation as a source of sheltering is impossible in this case as well for the reasons given earlier. It can be further remarked that separation is caused by a sustained adverse pressure gradient. Pressure gradients are present in this case, of course, but at any one spot they alternate rapidly between favorable and adverse.

The wall pressure distribution for a turbulent boundary layer over a standing wave is given by the appropriate superposition of the traveling wave pressure distributions as represented by Eq. (28) only with the free stream velocity given as $\frac{1}{2}U_\infty$. The resulting expression is

$$p_o - p_\infty = -\left[1 + \left(\frac{U_\infty}{2c}\right)^2\right]\rho(2\pi f)^2 \frac{a\lambda}{2\pi} \sin k\xi \sin kct$$

$$+ \frac{U_\infty}{2c} \rho(2\pi f)^2 \frac{a\lambda}{2\pi} \cos k\xi \cos kct \qquad (31)$$

III. CHARACTERISTICS OF A VIBRATING PLATE

The behavior of a plate vibrating with transverse standing waves can be analyzed by the classical theory of vibrations in elastic beams. The phenomenon can be thought of as characterized by the interaction of the inertia forces due to the mass of the plate with the elastic forces due to bending of the plate. When the plate forms the boundary of a fluid the inertial effects of the fluid must also be considered. In the case of liquids the elasticity of the fluid is ordinarily negligible.

When an infinitely long plate of unit width and depth d is vibrating with simple harmonic standing waves of amplitude a, wave length λ, and frequency f the inertial force due to the mass of the beam is given by

$$F_i = S\rho da(2\pi f)^2 \sin \frac{2\pi x}{\lambda} \cos 2\pi ft \qquad (32)$$

where ρ is the density of water and S is the specific gravity of the material of the beam. The distribution of wall pressure for the case of a standing wave with no flow is given in Fig. 2 to be

$$p_o = -\rho \frac{\lambda}{2\pi} a(2\pi f)^2 \sin \frac{2\pi x}{\lambda} \cos 2\pi ft \qquad (33)$$

The negative of the pressure may be thought of as the inertial force of the water per unit of plate area. The negative is required since positive pressures exert forces opposite in direction to y. Equation (33) holds for cases with flow provided U_∞/c is small as seen in Eq. (31). Comparison of Eqs. (32) and (33) shows that the term $\frac{\lambda}{2\pi}$ corresponds to d. The effect of the fluid is therefore to augment the mass of the plate by the mass of a layer of water of depth $\frac{\lambda}{2\pi}$. The frequency of vibration can now be computed using the classical theory (see, for example, Timoshenko [8], page 331.) to give

$$f = \frac{2\pi}{\lambda^2} \sqrt{\frac{Ed^3}{12(\rho Sd + \rho\lambda/2\pi)}} \qquad (34)$$

where E is Young's modulus of elasticity. Equation (34) can be put in more useful form using the relationship $c = f\lambda$ to give, in terms of d/λ, the relationship

$$c = 2\pi \frac{d}{\lambda} \sqrt{\frac{E}{12\rho S(1 + \lambda/2\pi dS)}} \tag{35}$$

Figure 3 shows a plotting of wave celerity versus the ratio d/λ based on Eq. (35). The physical constants were evaluated for steel and water. The term for the added mass of the water is included in the lower curve but neglected in the upper curve. This chart emphasizes the strong dependence of wave celerity on the stiffness of the plate.

The above remarks apply to plates or beams infinitely long. A plate of finite length, however, pin supported at its ends, will vibrate as an infinitely long plate with nodes located at the supports. The reason is that an infinitely long plate has zero bending moment and maximum shear at the nodes as should occur at a pin-supported end. A given plate will have a number of modes of vibration. The fundamental mode with only one loop is worse from the point of view of this study since it has the lowest equivalent wave celerity. A plate of length L vibrating in its fundamental mode will have a wave length of 2L.

Practical aspects of design naturally limit the slenderness of actual plates and by doing so limit the equivalent wave celerities c of resonant standing waves. The midspan deflection Δ of a uniformly loaded beam, simply supported at its end, is given by the expression

$$\frac{\Delta}{L} = \frac{w}{E} \frac{60}{384} \left(\frac{L}{d}\right)^3 \tag{36}$$

where w is the loading per unit length. For example, steel plate loaded with one atmosphere of pressure will have a $\frac{\Delta}{L}$ ratio of about 0.01 for an L/d ratio of 50. The corresponding wave celerity is 175 fps. For a L/d ratio of 100 the $\frac{\Delta}{L}$ ratio is 0.08 and the corresponding wave celerity is 72 fps. The latter values of sag seem far beyond the limits of acceptable design.

The steepness of standing waves is also limited by design conditions. Figure 3 shows the relationship between the d/λ ratio and the wave

steepness ratio a/λ as governed by two different design criteria. The first is the "extreme fiber stress" in the deflected plate and the second is the fluctuation in wall pressure. The wave steepness as related to plate thickness is shown, by way of example, for an extreme fiber stress of 20,000 psi, a common structural value. This curve shows that except for extremely flexible plates the wave steepness is restricted to the order of 1 per cent or less. The other curve on this chart shows the wave steepness that will cause a pressure fluctuation of plus and minus one atmosphere. For this condition cavitation would occur at the loops if the reference pressure is atmospheric. This limitation is seen to be very severe for the larger d/λ ratios.

IV. EXPERIMENTAL PROGRAM

The purpose of the experiments was to determine whether or not standing wave vibrations on a smooth boundary plate would disturb a turbulent boundary layer sufficiently to cause an extra induced drag. It was recognized that the method of testing must be such that an effect would be detected even if it were very small. It was necessary that the measurements be as fundamental and direct as possible in order that the turbulence of the flow and the vibrations in the tunnel would not mask the overall effect that was sought. It was impossible to attach any instrument to the plate itself as the vibrations of the plate would make the readings meaningless. Wall shear measuring devices such as a shear plate dynamometer or a shear tube of the preston type were considered for location just downstream of the plate. But it has been reported that the wall shear adjusts itself very rapidly to the boundary conditions so that the effect of the vibrating plate upstream would not likely be sensed by such devices.

The effect of vibration on the boundary layer is measured most directly and completely by velocity traverses taken upstream and downstream of the vibrating section. Comparison of these velocity profiles for the different conditions of vibration provides an immediate test for the presence of any effect. Furthermore, introduction of this data into the momentum equation would provide a quantitative estimate of the change in drag. It is important, of course, that this data be very accurately measured and that all extraneous effects be reduced to a minimum.

V. TEST APPARATUS

The apparatus on which the experiments were performed is shown diagrammatically in Fig. 4. Figure 5 contains photographs of the equipment as well. The vibrating plate water tunnel, fabricated for this research, is a modification of a permanent facility of the Laboratory. Prior to alteration, the water tunnel consisted of a 12 in. by 18 in. rectangular test section drawing water from a vertical stilling tank 10 ft high and 4 ft in diameter. The tank is supplied from the Mississippi River by a 12 in. diameter penstock with a control valve at the inlet to the tank. The pressure in the tunnel was controlled by a throttling gate at the discharge end. The portions of the earlier tunnel used in the present facility are shown in bold lines in Fig. 4.

It is essential in boundary layer studies that the turbulence of the incoming flow be as low as possible. The stilling tank provided was actually too small for its purpose considering that there is a 40-ft pressure head on the penstock which jets water into the tank at 50 fps. The cross-sectional area of the tunnel was changed to 12 in. by 8 in. to reduce the discharge required and make the tank more effective. Screens and flow straighteners were provided to reduce the turbulence further to a seemingly acceptable level.

The actual tunnel, constructed of lucite, was made with a cross-section 12 in. square. The upper 8 in. of depth formed the tunnel proper. The lower 4 in. was separated by a slotted wall to form a plenum chamber with its own pressure control. The plenum chamber had two purposes. One was to provide some control over the longitudinal pressure gradient in the tunnel and the other was to increase the depth of the tunnel to the order of $\frac{1}{2}\lambda$ so that fluctuating pressures and velocities would be negligible at the lower wall.

The condition of zero pressure gradient along the wall requires, of course, a constant core velocity. The effect of the boundary layer is to reduce the effective cross-section dimensions of the tunnel by the amount of the displacement thickness, causing the core velocity to increase. Discharge must therefore be bled off through the slotted wall as the boundary layer displacement thickness increases. The slot discharge per unit of wall area

is proportional to the free stream velocity and the lengthwise rate of increase of the displacement thickness. The rate of increase of the displacement thickness is approximately proportional to the distance from the leading edge to the power of - 1/5. (See Schlicting [6], page 432.) The slotted portion started 21 in. downstream of the leading edge of the transition and extended for 5 ft of the tunnel. Thus the required slot discharge was highest at the upstream end and tapered off slightly downstream.

The slot discharge per unit area of wall is proportional to the slot velocity and the slot porosity. The velocity through the slots is controlled by the pressure drop across them. The slot velocity at different points along the wall is influenced by lengthwise variations in the pressures in the main tunnel and in the plenum chamber. The pressure variations in the plenum were minimized by making the chamber sufficiently large so that the velocity heads associated with the plenum flow were everywhere negligible. The effect of pressure variation in the main flow can be minimized if the pressure drop across the wall is of a much larger order of magnitude than the variations. A good criterion is that the velocity through the slots be made equal to the main flow velocity. Then, assuming the slots as orifices, a 1 per cent variation in tunnel pressure will produce only 0.5 per cent variation in slot velocity.

With the slot velocity equal to the main stream velocity the proper distribution of slot discharge is accomplished if the porosity varies directly with the rate of growth of the displacement thickness. On the basis of preliminary calculations a slot porosity distribution was used with porosities ranging from 0.0055 upstream to 0.0045 downstream.

The vibrating portion of the tunnel was a stainless steel plate 12 in. wide, 45 in. long, and 1/8 in. thick, composing part of the upper wall. It was mounted completely independent of the tunnel and connected to it only by a very thin flexible plastic seal. The plate was supported at each end by a heavy structural steel frame fastened directly to the basement floor of the Laboratory. Special care was required to align the ends of the plate to the remainder of the lucite upper wall to insure that there would not be a vertical discontinuity in the upper boundary and that there would be no physical contact with the rest of the tunnel. The end supports were pin connected so that the plate would vibrate naturally as an infinite plate with nodes at the ends. The nodes are points of zero bending moment but maximum shear.

The supporting frame had to be rigid enough to withstand the large vertical harmonic end reactions supplied by the plate and to give a minimum of vertical displacement.

A 1/8 in. thick plate, 45 in. long, has little resistance to internal pressure. Two intermediate vertical restraints were provided to keep the plate from bulging out of its plane. Their position was adjustable so that they could be located at intermediate nodal points. Even so, the internal pressure had to be carefully controlled. This was accomplished by a head loss gate at the discharge end.

Various types of electronic, electro-mechanical, and mechanical vibrators were investigated before deciding on the type adopted for these tests. The exciter used was a pneumatic vibrator manufactured by the Martin Engineering Company of Neponset, Illinois under the trade name "Vibrolator". A portion of one is shown in one of the photos of Fig. 5. It consists simply of an enclosed circular raceway on which a steel ball is free to roll. A jet of high velocity air strikes the ball once each revolution to maintain its circular motion. The vibrator transmits a two-directional harmonic vector force to any object on which it is bolted. In the apparatus the vibrator is mounted to the vibrating plate at mid-span through a linkage arrangement that transmits only the vertical component of the vector force. The vibrator is suspended from the supporting frame by low tension springs which counterbalance the weight of the vibrator and the plate but transmit little of the vibrational force to the frame.

This type of exciter has several advantages over the others investigated for this program. It is a great deal more compact and far less expensive than electronic exciters and has the further advantage that the vector force increases with the frequency of vibration instead of decreasing as is the usual case. In addition it provides a pure harmonic force with a frequency that is controlled simply by adjusting the air pressure. Its main drawback is that the vector force is dependent entirely on the frequency. This shortcoming can be avoided by using a series of vibrators, each with a different vector force-frequency relationship.

Only two models in the Vibrolator series were used in these experiments. One was the model CV35 which had a 0.383-lb ball and a raceway providing a 0.625-in. eccentricity to the center of gravity. The vector force

for this model is 240 lb at 100 cps. The other model was the CV19 with a 0.0622-lb ball and a 0.688-in. eccentricity. Its vector force at 100 cps is 43 lb. The vector force varies with the square of the frequency.

The vibrational displacements of the plate were measured with a simple displacement meter designed at the Laboratory employing a linear variable differential transformer produced by Schaevitz Engineering of Camden, New Jersey. The output of the meter was fed to a paper strip pen recorder and a cathode tube oscilloscope. The pen recorder was most useful for measuring frequencies and the oscilloscope for measuring displacement. The oscilloscope was also very useful for observing the shape of the wave with respect to time.

A series of flattened stagnation tubes with varying tip dimensions were fabricated in order to measure the boundary layer velocities. The dimensions of the tubes are shown in Fig. 6. All but one of the tubes were made from 1/8-in. diameter stainless steel tubing with a 1/16-in. internal diameter. The smallest tube of the series, however, had a tip made of 1/16-in. stainless steel tubing with a 1/32-in. internal diameter. The wall thickness at the tip was reduced to 0.002 in. and the tip was flattened to a thickness of 0.0085 in. The stems of all the tubes of the series were made from 1/4-in. diameter stainless steel tubing.

Glands were provided in the upper wall at three stations for insertion of the stagnation tubes. The gland for Station 1 was 2 in. upstream of the plate, for Station 2 was 6 in. downstream of the plate, and for Station 3 was 12 in. downstream of the plate. Station 3 was used only for measuring the core velocity. The actual measurements were, of course, taken at the tip of the stagnation tube, which is 2.5 in. upstream of the stem portion.

A dial gage set against a block clamped to the stagnation tube stem was used to measure the distance of the probe from the wall. In addition, a gold-plated electrical contact was set flush into the upper lucite wall just over the stagnation tube tip. An electric circuit was set up so that a light turned on when the probe just touched the wall. This system proved very sensitive and provided accurate readings for the traverse distance.

The static pressure required for the determination of the velocity heads was measured by two wall taps, each located on the upper wall two inches

on either side of the centerline at the same longitudinal section as the stagnation tube tip. Additional wall taps were installed along the back wall at mid-depth in the 8-in. channel in order to survey the longitudinal pressure profile.

VI. TEST RESULTS

The measurements describing the modes of vibration of the plate are shown on Fig. 8. The plate could be made to vibrate with almost a continuous range of frequencies by adjusting the pressure of the compressed air driving the exciters. However, except for three resonant conditions the oscillations were very small and usually negligible except under the exciter. Careful tuning to the resonant conditions produced the very good vibration patterns shown in Fig. 8. Once tuned, the vibrator frequency would lock in phase and remain stable even for fairly substantial changes in air pressure. Data are shown for core velocities of 2.4 and 15 fps.

Resonance with three loops and with five loops was obtained with the larger of the two vibrators. The frequencies for the two conditions are 14.8 cps and 57 cps and the amplitudes under the exciter are 0.050 and 0.011 in. Only the seven loop resonance was obtained with the smaller vibrator. The frequency and amplitude for this condition are 122 cps and 0.004 in. The amplitude of the different loops along the plate can be seen to vary. This is due largely to the concentrated mass of the exciter mount and to a lesser degree to the conditions at the end supports where some movement was observed.

The wave pattern with respect to time is shown in Fig. 8 on photographs of portions of the pen recorder paper. The higher frequencies are approaching the limit of the recorder but the sinusoidal character of the wave is clearly evident. The pen tracings have been retouched in spots to improve the reproduction for the report. The frequencies reported were measured with this recorder but the amplitudes were obtained from oscilloscope patterns.

The variation in amplitude along the plate caused slight variation in wave length, but the nominal values are 30, 18, and 12 6/7 in. The corresponding values of wave celerity c are 36.9, 85.5, and 133 fps and the d/λ values for the 1/8-in. plate are 0.0042, 0.0074, and 0.0096. The wave celerity data are plotted on the chart of c versus d/λ on Fig. 3. The

points are seen to lie below the theoretical line. The difference is probably attributable to the added mass of the exciter mount. Also plotted on Fig. 3 are the wave steepness values, 0.0016, 0.00061, and 0.00031.

The pressure distribution along the tunnel was controlled by the flow through the slotted wall and the plenum chamber as controlled by the downstream pressure control gate. In the early exploratory tests of the program a slotted wall was used which had a relatively high porosity. During the tests it was observed that flow passed through the slotted walls into the plenum chamber in the upstream region but in the reverse direction in the downstream region. As a result the main stream velocities decreased in the upstream portion and increased again downstream. Correspondingly, the pressure gradient was strongly negative upstream and positive downstream.

For the tests documented in this report a slotted wall of much lower porosity was used. The design of the wall was in accordance with the remarks made earlier on slotted walls. The porosity was made low enough so that the slot velocity approximates the core velocity. The porosity was also varied in the lengthwise direction in proportion to the calculated variation in the rate of displacement thickness increase. During a test the pressure in the plenum chamber was adjusted until the piezometer tubes showed a minimum pressure variation in the tunnel.

Figure 9 shows the readings for the optimum settings for the three standardized flows: 2.4 fps, 6.0 fps, and 15 fps. The reference pressure used for these plottings is the average of all the readings for any given condition. The variation of pressure head along the channel is mostly less than plus or minus 1 per cent of the main stream velocity head. Without a slotted wall the rise in pressure head for this length would be about 6 per cent of the velocity head. The pressure head drop across the slotted wall for optimum conditions was measured to be 0.24 ft, 0.65 ft, and 2.44 ft for the 2.4, 6.0, and 15 fps core velocities. The slot velocities corresponding to these heads are 3.9, 6.5, and 12.2 fps or 1.62, 1.08, and 0.81 times the respective core velocities.

Figure 9 presents pressure distribution data for the four vibration conditions (including zero frequency). The plenum pressure was adjusted to optimum for each flow condition but was kept the same for all the frequencies for each flow so that any influence of frequency on the pressure would be

detected. The data indicate that no measurable influence existed for these conditions.

The most important results to be presented from this program are the boundary layer velocity profiles on Figs. 10, 11, and 12. Figure 10 shows the velocities taken at Stations 1 and 2 for a flow having a free stream velocity of 2.4 fps. Figure 11 contains the data for a free stream velocity of 6.0 fps and Fig. 12 for 15 fps. Data on the four vibrational conditions are given for each flow for Station 2, but only zero frequency data are given for Station 1 upstream. It must be stated at the start that the results show no measurable influence of vibration even though the data cover values of c/U_∞ from 55 to 2.5.

Conditions in the tunnel made it very difficult to obtain consistent data. The main source of difficulty was a very low frequency, irregular pressure surge that made manometer reading very difficult. Several unavoidable factors seemed to contribute to this. These included surges in the 300 ft long supply channel, pressure pulses in the approximately 100 ft long penstock, and air accumulation from air precipitation in the region of subatmospheric pressure immediately downstream of the intake valve. Dampening in the manometer system was ineffective and electronic sensing devices that were tried were not accurate or consistent enough.

The method finally resorted to was to use straight half-inch glass piezometers and photograph the fluid levels fifty times for each setting at 1 sec intervals using a 16 mm movie camera. Each movie frame showed four piezometer tubes. The tube to the left was connected to the wall static tap in the tunnel roof, located 2 in. to the left of the centerline at the measuring section; the second from the left was connected to the boundary layer stagnation tube; the third was connected to the main stream stagnation tube at Station 3 and the last was connected to the wall static tap to the right of the centerline. The movie frames were read on a microfilm viewer against an arbitrary scale attached to the ground glass. The results were typed directly onto punched tape for electronic computing. The computer calculated the u/U_∞ ratio for each frame and gave the mean value and standard deviation for the fifty frames for each setting. Settings with suspiciously high standard deviations were rerun and the values with the lowest standard deviation was used. With proper lighting the meniscus was very well defined and good results were obtained using telephoto lenses even for the low flows.

The data in Figs. 10, 11, and 12 are plotted in the most fundamental form possible for several reasons. First, this plotting is sufficient for the purpose of the report, namely to demonstrate the effect of vibration. Second, this fundamental form is most convenient for others who may wish to replot it in any way. Third, the dimensionless plots require the use of parameters such as shear velocity, boundary layer thickness, and distance from the leading edge that were not conducive to accurate measurement. There also have been no corrections applied to compensate for the presence of the wall, the velocity gradient, turbulence intensity, and/or laminar effects at the tip of the probe. All the data shown were taken with the smallest stagnation tube, which has a thickness of 0.0085 in. A correction of + 0.004 in. was made to the dial gage reading to account for the semidiameter.

The results are, however, in fairly good agreement with that of other researchers. In Fig. 10 the data for y greater than about 0.04 in. can be fitted almost exactly to the logarithmic law

$$\frac{u}{V_o^*} = 5.85 \log \frac{V_o^* y}{\nu} + 5.56 \qquad (37)$$

which was suggested by Nikuradse's measurements (see Schlicting [6], page 437.) provided values of V_o^* of 0.126 and 0.113 fps are used for Station 1 and Station 2 respectively. For y less than 0.04 in. the data fall away from this curve and follow a transition curve leading to the laminar sublayer (see Schlicting [6], page 405).

Station 1 and Station 2 are 1.46 and 5.80 ft downstream from the leading edge of the tunnel transition measured horizontally. The temperature of the water during the tests varied between 43° and 45° F. The Reynolds number based on distance from the leading edge, is 0.25×10^6 for Station 1 and 1.00×10^6 for Station 2. Schlicting [6], p. 438, presents values of the local drag coefficient c_f' as a function of Reynolds number for the velocity profile in Eq. (37). The shear velocity easily follows and calculates to be 0.117 and 0.105 fps for Stations 1 and 2. These values are both very nearly 7 per cent lower than the ones obtained from the curve fitting process. This is not unreasonable considering the state of the art of measuring wall shear at the time these equations were evaluated.

Figure 11 shows the measured velocity profiles at Station 1 and Station 2 for a free stream velocity of 6.0 fps. The velocities fit Eq. (37) quite closely for values of y between about 0.01 and 0.1 in. when values of shear velocity of 0.285 and 0.251 fps are used. The Reynolds numbers at these stations, completed as above, are 0.62×10^6 and 2.47×10^6 and the corresponding values of shear velocity from Schlicting are 0.270 and 0.239 fps. The discrepancy for this flow is about 5 per cent. For values of y greater than 0.1 in. the velocities are greater than given by Eq. (37). In this region the velocity profile fits the 1/7th power law much better.

Figure 12, which contains the measured velocity profiles for a core velocity of 15 fps, fits Eq. (37) well for y less than 0.04 in. and the 1/7th power law for y greater than 0.04 in. The shear velocities obtained from the curve fitting are 0.668 and 0.583 fps for Stations 1 and 2. The Reynolds numbers are 1.55×10^6 and 6.20×10^6 and the corresponding shear velocities from Schlicting are 0.624 and 0.556 fps.

The data on Fig. 12 are the most interesting from the point of view of the study because the 15 fps flow has the lowest wave celerity to core velocity ratio. The ratio has values of 2.46, 5.70, and 11.3 for the 14.8, 57, and 122 cps vibrations. These values are within the range where the viscous part of the velocity disturbance starts to extend beyond the laminar sublayer. The data, nevertheless, show that the mean properties of the boundary layer are unaffected by the vibration.

VII. CONCLUSIONS

From the theory presented it is possible to conclude:

(1) A turbulent boundary layer passing over a smooth plate vibrating with low amplitude standing waves receives a harmonic disturbance that can be resolved into two additive components, an inviscid motion and a viscous motion, both of which decrease exponentially with distance from the wall.

(2) The viscous motion decreases very rapidly with distance from the wall and is largely contained within the laminar sublayer provided the wave celerity c is greater than 3.5 times the free stream velocity.

(3) The inviscid motion has very low velocity gradients and becomes negligible at a distance of 0.7λ from the wall.

(4) A sheltering effect is possible if the inviscid motion becomes out of phase with the wave form.

(5) The boundary condition of the viscous motion governs the relationship of the inviscid motion to the wave form and is such that there is no sheltering effect, provided that c is greater than 3.5 times the free stream velocity.

(6) The sheltering effect if any is a function of the wave celerity and the free stream velocity and does not depend directly on wave amplitude, wave length, or wave frequency.

From an inspection of the properties of plates presented in the report it is possible to conclude:

(1) Stiffness requirements for any conceivable structural purpose limit the possible amplitude of vibration to well within the applicability of the theory.

(2) Stiffness requirements also limit the possible wave celerities to the order of 100 fps or greater.

From the experimental data it is possible to conclude that standing waves have no measurable influence on the boundary layer for any conditions tested, even though the vibrating plate was well over 50 boundary layer thicknesses long and the wave celerity to free stream velocity ratio was tested as low as 2.54.

LIST OF REFERENCES

[1] Benjamin, T. B. "Shearing Flow Over a Wavy Boundary", Journal of Fluid Mechanics, Vol. 6, Part 2, August 1959, pp. 161-205.

[2] Miles, J. W. "On the Generation of Surface Waves by Shear Flow", Journal of Fluid Mechanics, Vol. 3, Part 2, November 1957, pp. 185-204.

[3] Motzfeld, H. "Die Turbulente Strömung an Welligen Wanden", Zeitschrift für Angewandte Mathematik und Mechanik, Vol. 17, 1937, pp. 193-212.

[4] Krämer, M. O. "Boundary Layer Stabilization by Distributed Damping", Journal of American Society of Naval Engineers, Vol. 72, No. 1, February 1960, pp. 25-34.

[5] Benjamin, T. B. "Effects of a Flexible Boundary on Hydrodynamic Stability", Journal of Fluid Mechanics, Vol. 9, Part 4, December 1960, pp. 513-532.

[6] Schlicting, H. Boundary Layer Theory. Pergamon Press, London, 1955, 525 pages.

[7] Holstein, H. "Über die äussere und innere Reibungsschicht bie Störungen Laminar Strömungen", Zeitschrift für Angewandte Mathematik und Mechanik, Vol. 30, January-February 1950, pp. 25-49.

[8] Timoshenko, S. and Young, D. N. Vibration Problems in Engineering, D. Van Nostrand Company, New York, 1955, 468 pages.

[9] Dutton, R. A. The Velocity Distribution in a Turbulent Boundary Layer on a Flat Plate, Aeronautical Research Council C. P. No. 453, October 1957, 14 pages.

F I G U R E S

(1 through 12)

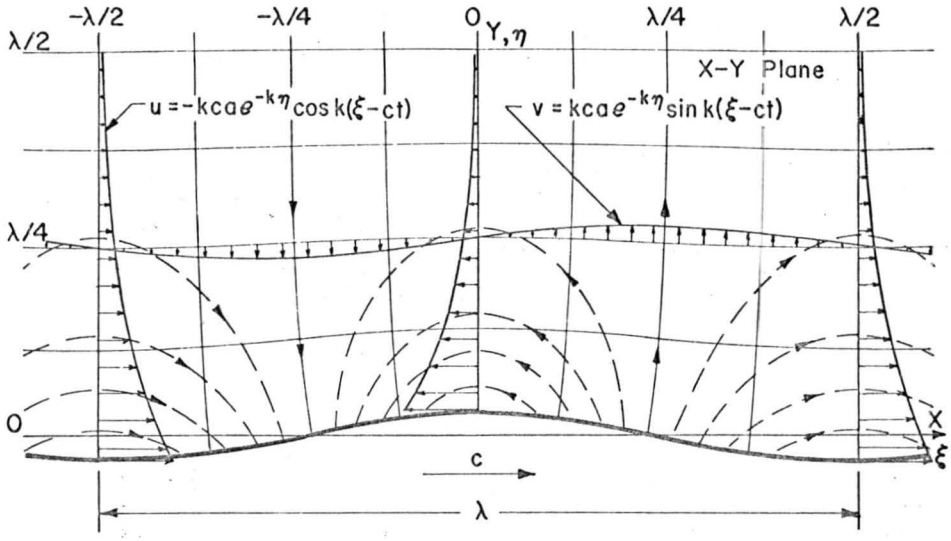

Potential Flow Pattern

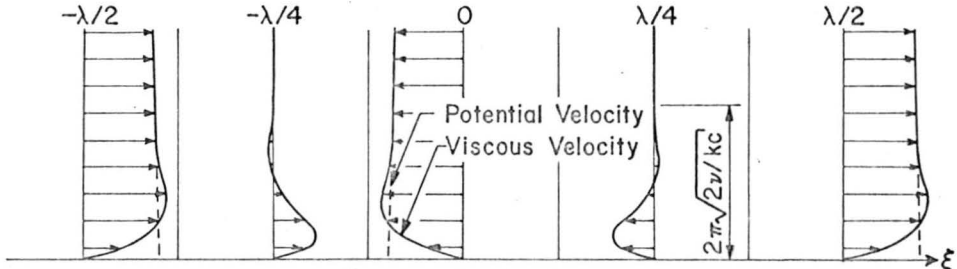

Viscous Flow Pattern
η Scale Greatly Magnified

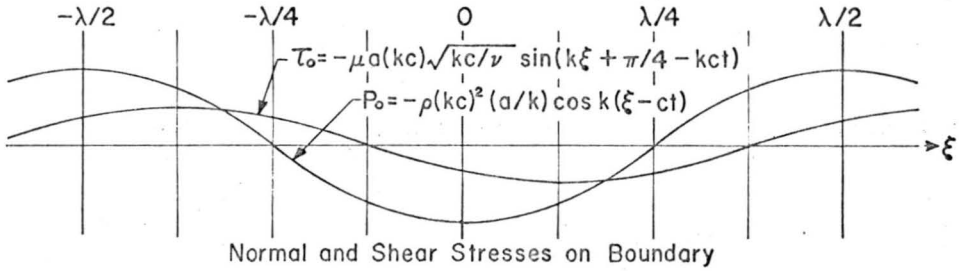

Normal and Shear Stresses on Boundary

Fig. 1 - Flow Characteristics for a Stationary Boundary with a Moving Sinusoidal Wave Pattern--No Main Flow

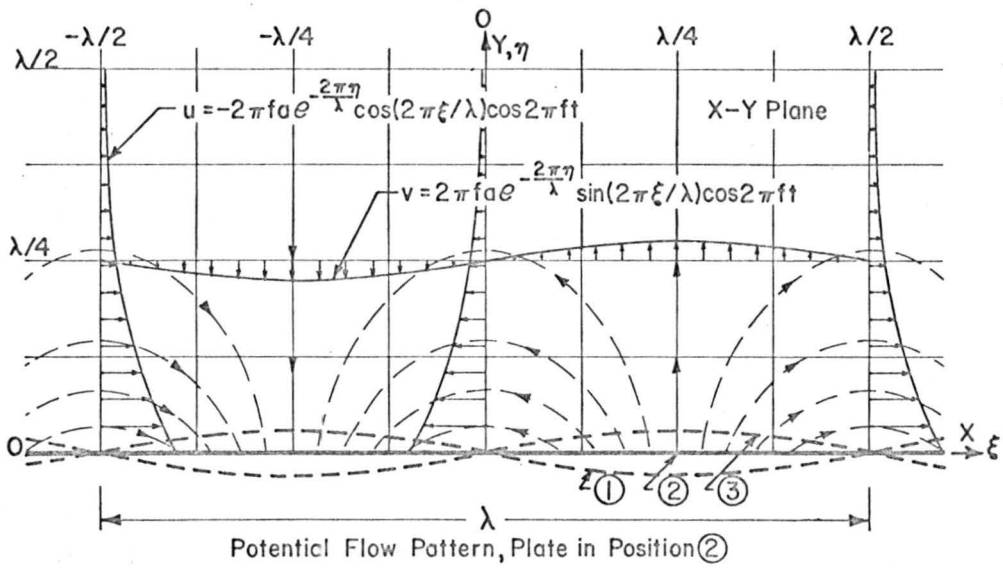

Potentiol Flow Pattern, Plate in Position ②

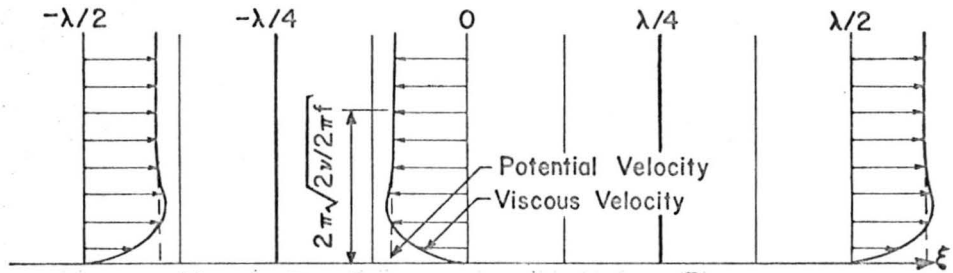

Viscous Flow Pattern, Plate in Position ②
η Scale Greatly Magnified

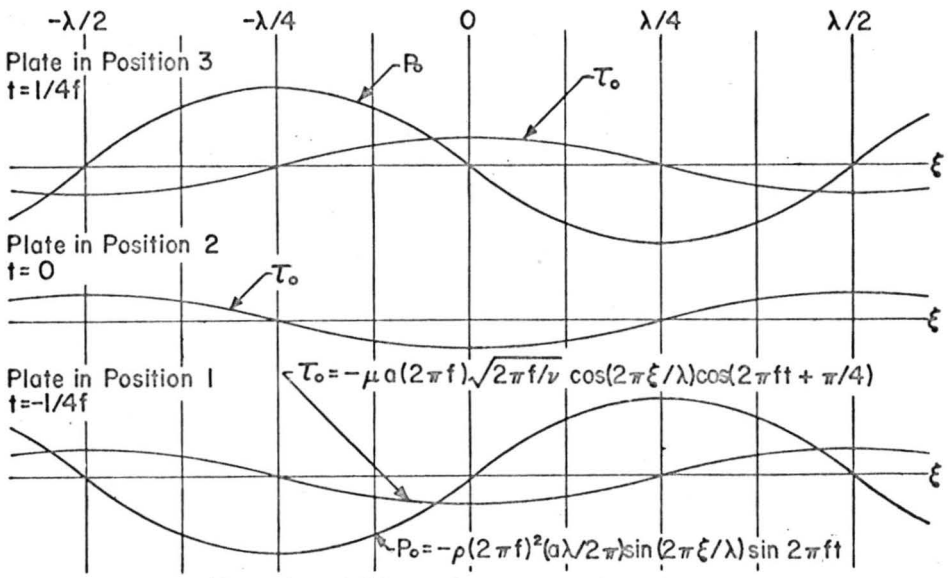

Normal and Shear Stresses on Boundary

Fig. 2 - Flow Characteristics for a Stationary Boundary with a Standing Sinusoidal Wave Pattern--No Main Flow

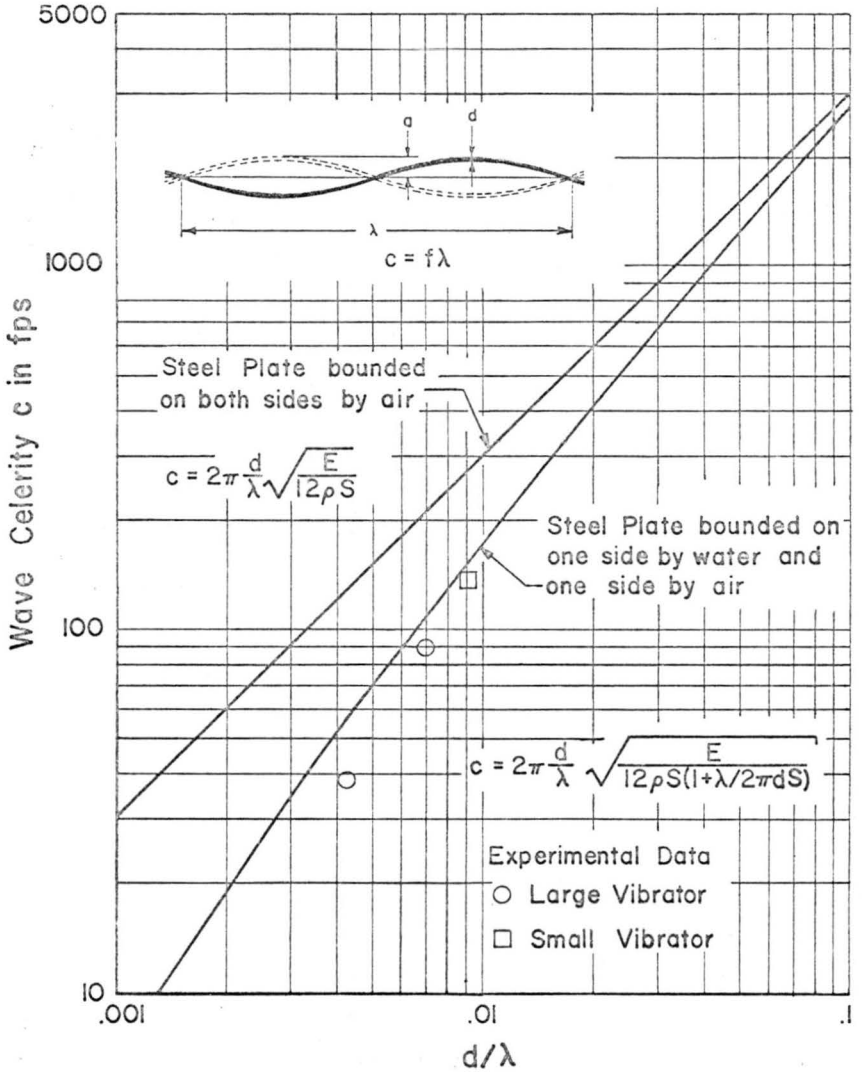

Effect of Plate Thickness on Wave Celerity

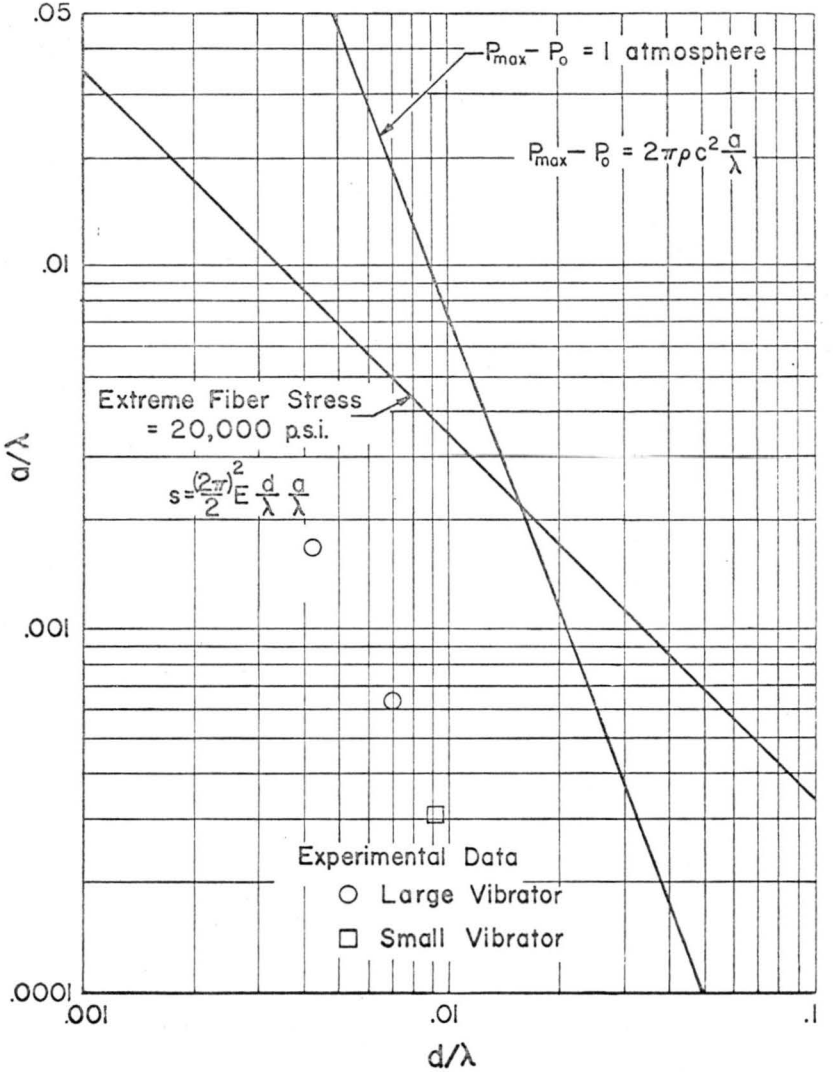

Wave Steepness for a Flexible Steel Plate

Fig. 3 - Vibrational Characteristics of a Flexible Plate

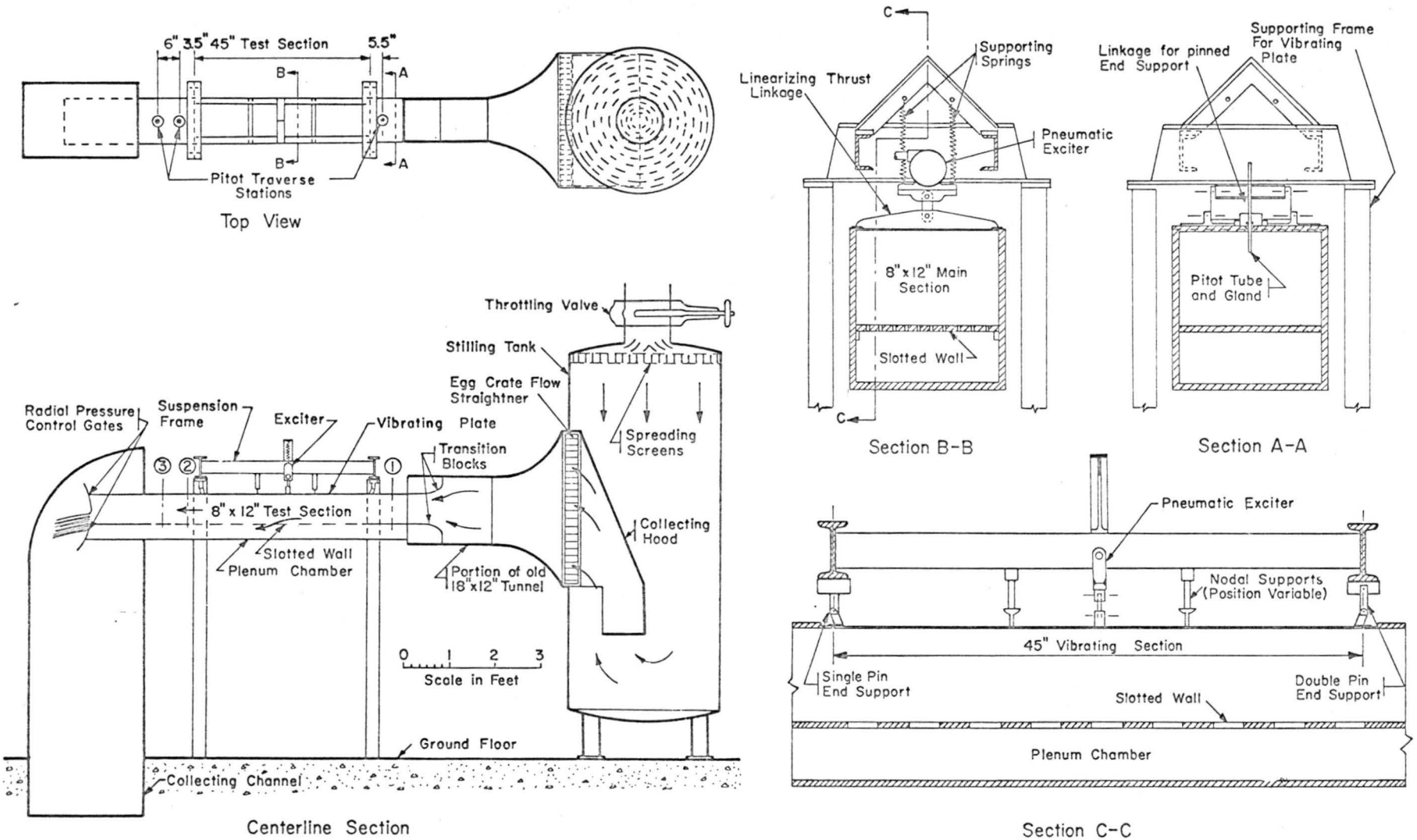

Fig. 4 - Apparatus for the Vibrating Plate Tests

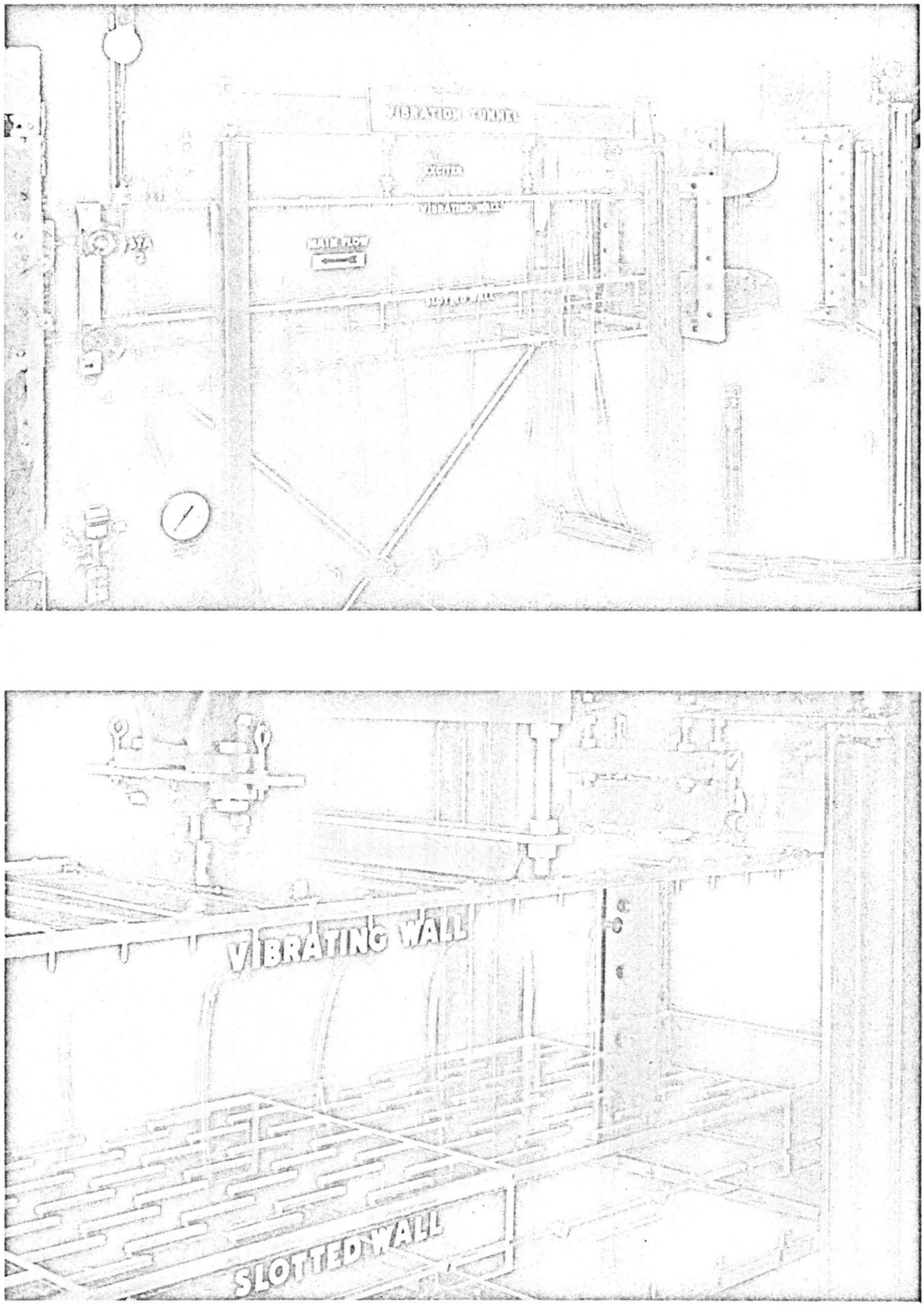

Fig. 5 – Photographs of the Test Apparatus

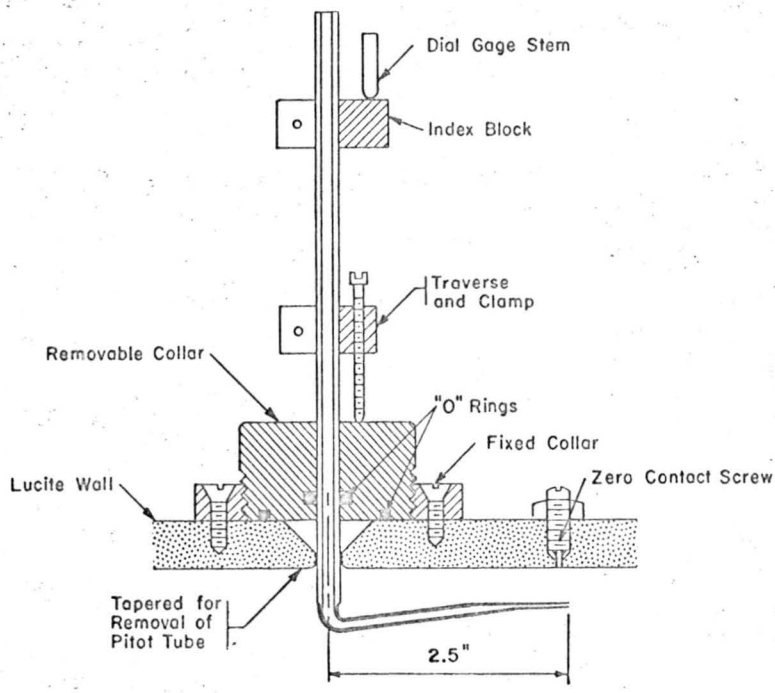

Pitot Tube Assembly

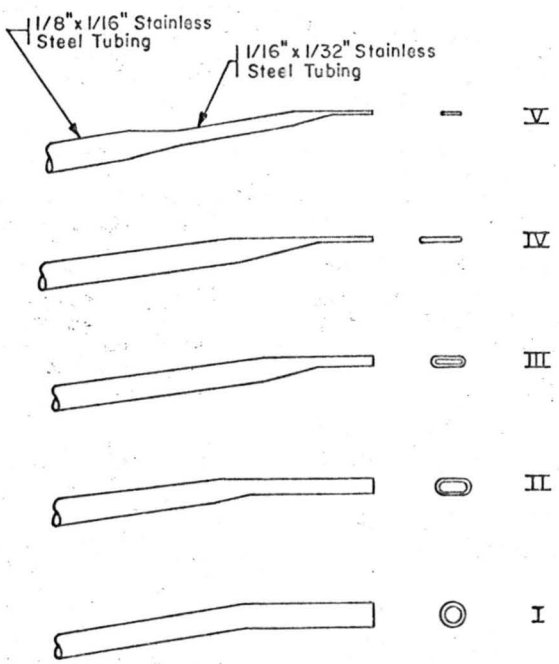

Pitot Tube Series

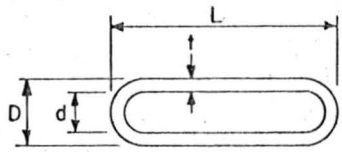

Entrance Cross Section

Type	L	D	d	t
I	Round	0.127	0.095	0.016
II	0.140	0.067	0.035	0.016
III	0.157	0.031	0.015	0.008
IV	0.154	0.016	0.008	0.004
V	0.076	0.0085	0.0045	0.002

Measured Dimensions in Inches

Fig. 6 - Boundary Layer Pitot Tubes and Assembly

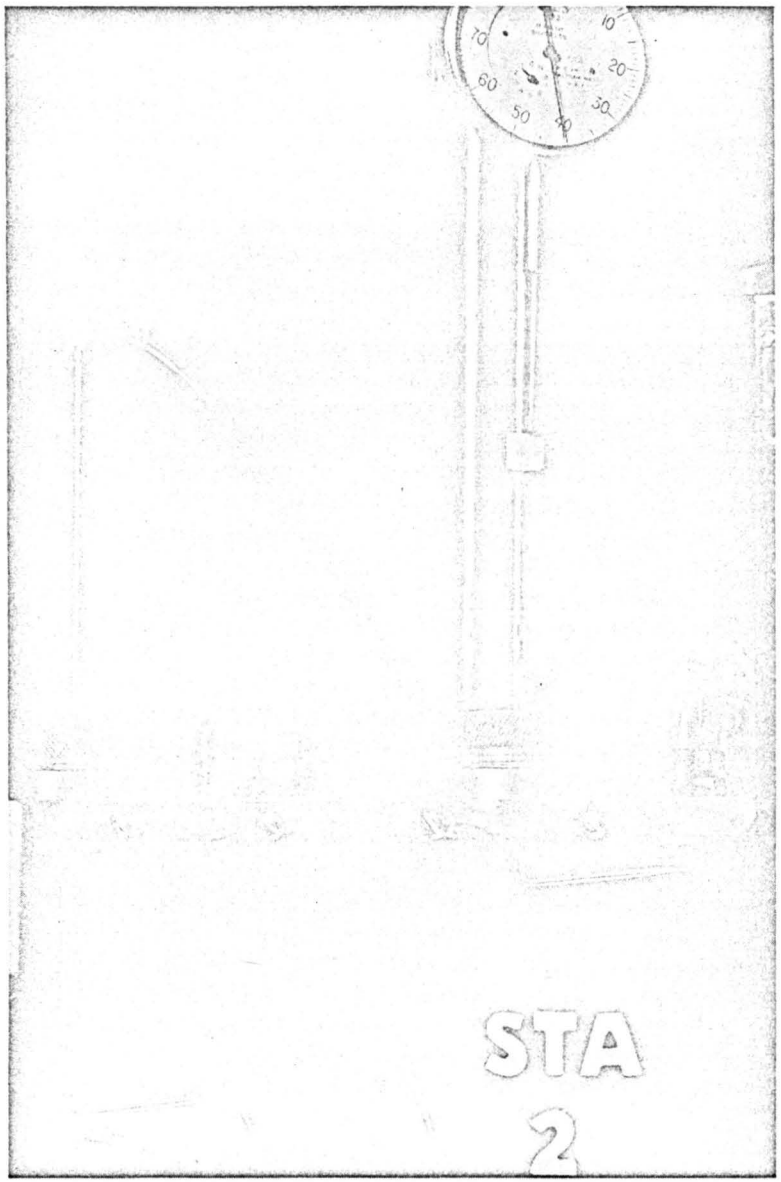

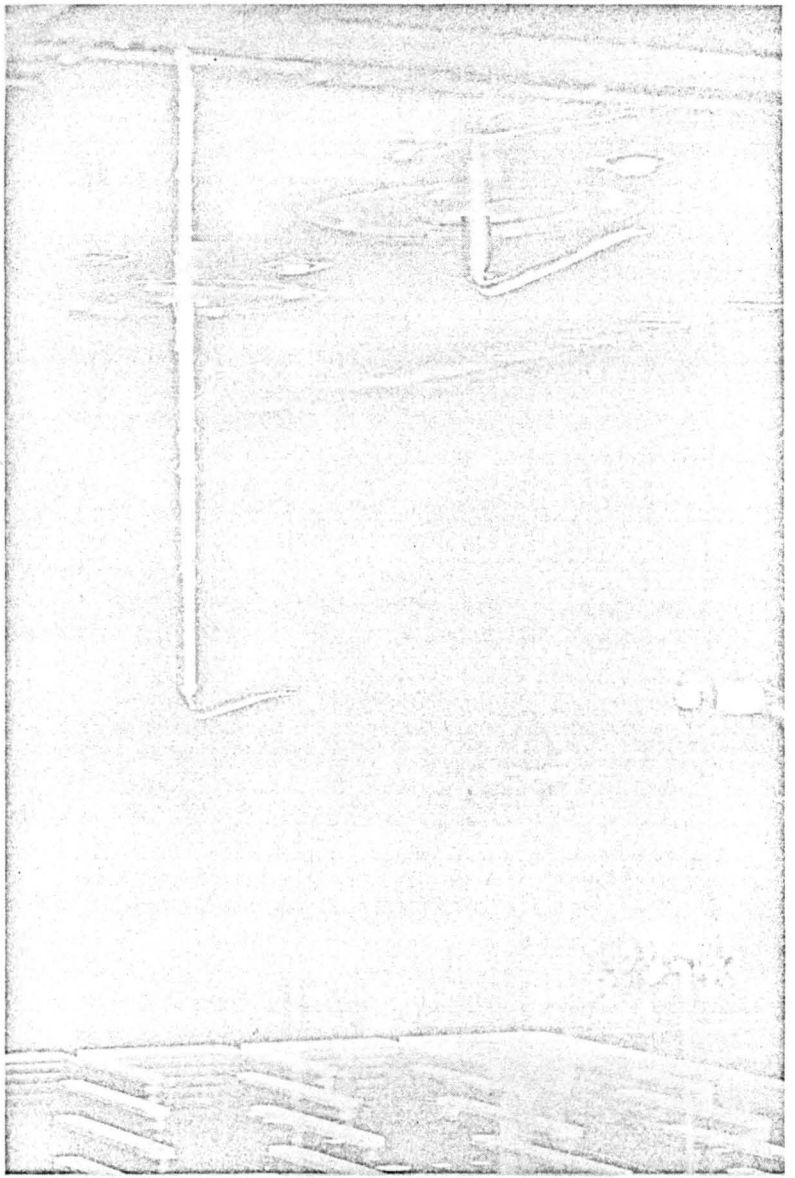

Fig. 7 - Photographs of the Boundary Layer Pitot Tube Assembly

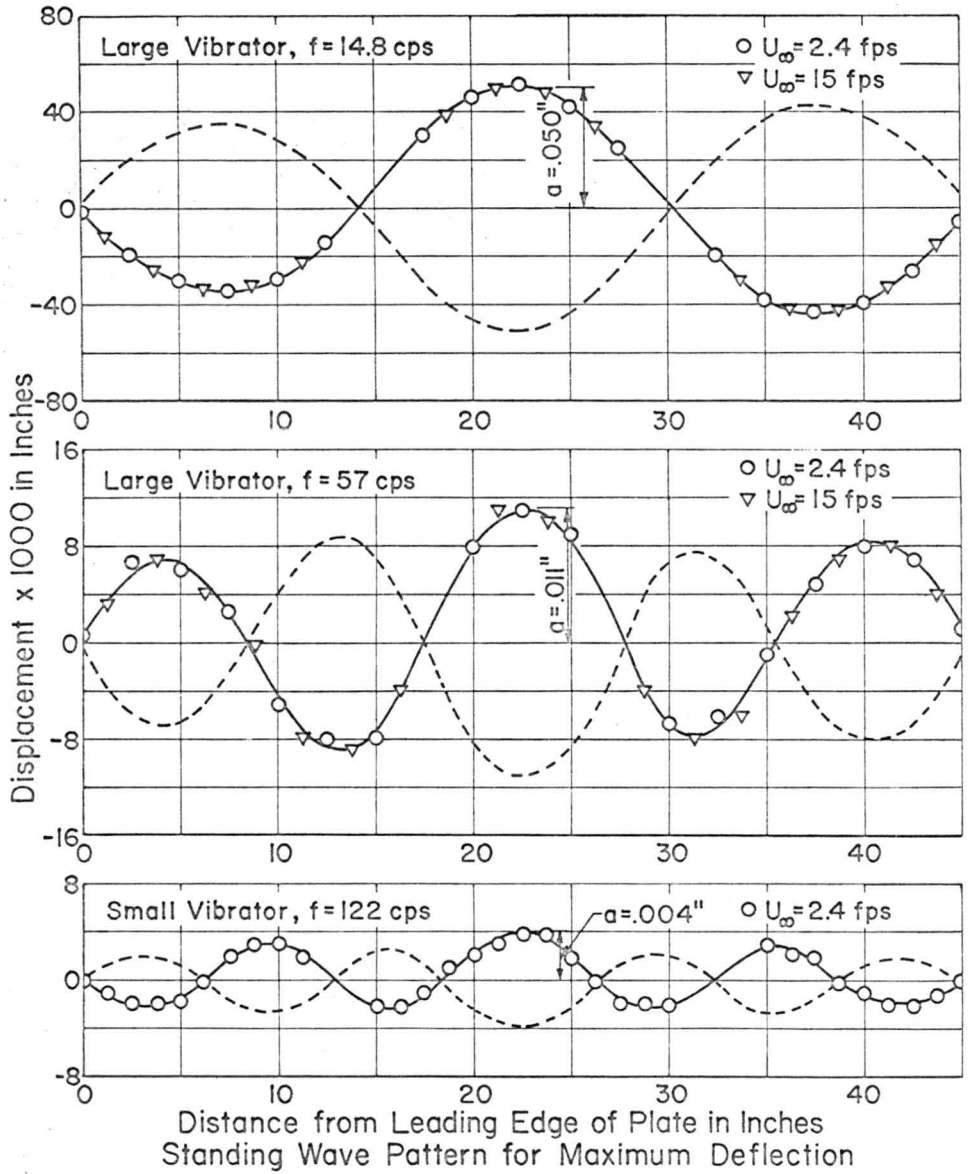

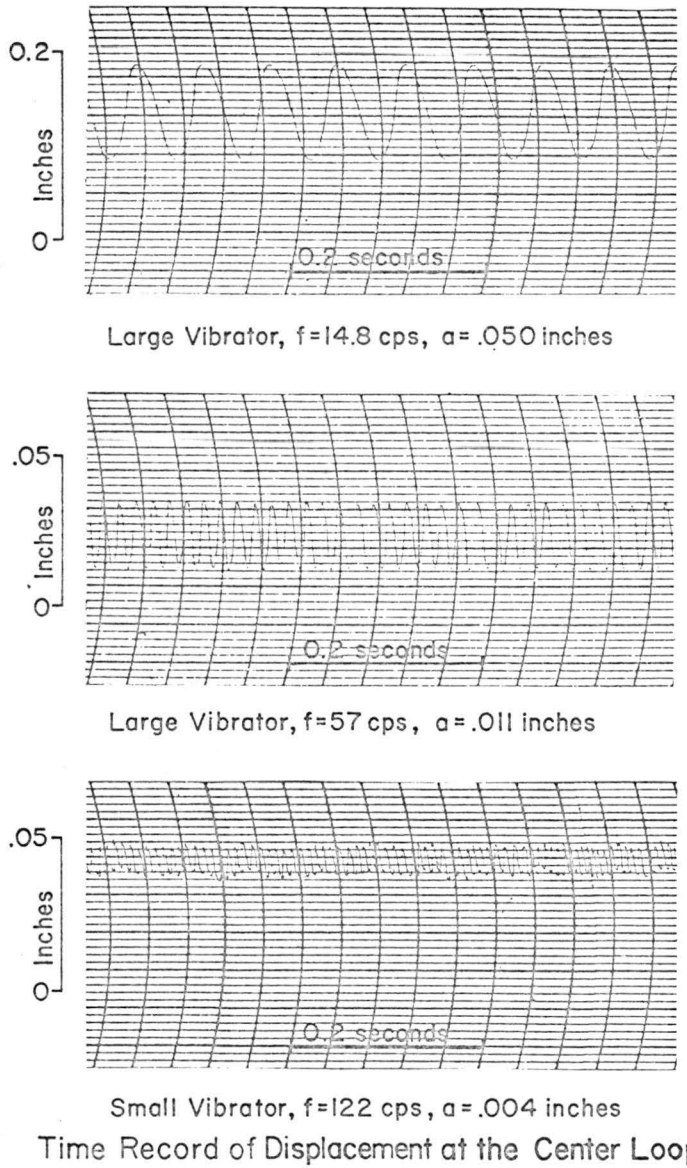

Fig. 8 - Measurements of Plate Vibrations

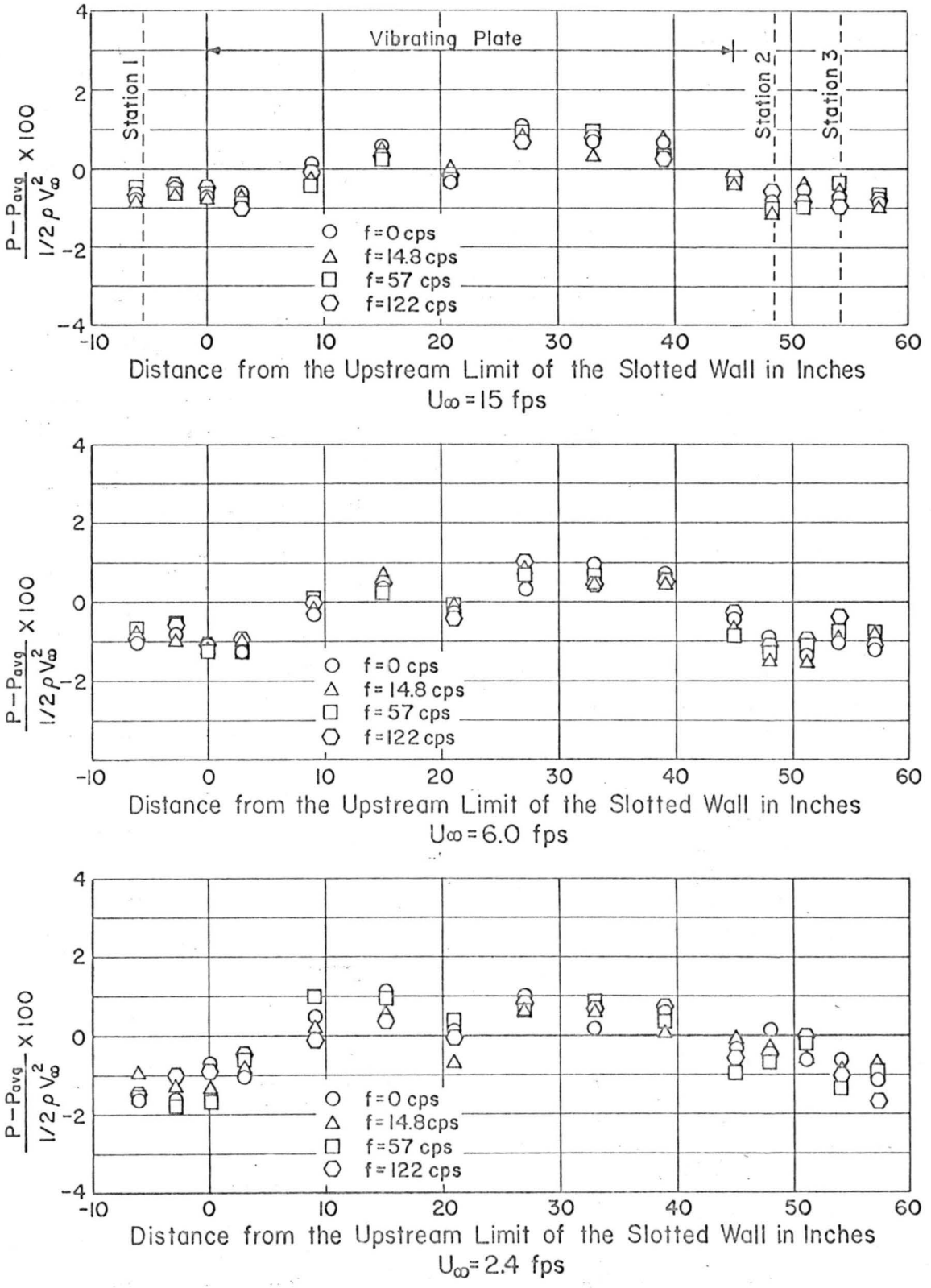

Fig. 9 - Measurements of the Longitudinal Pressure Gradient

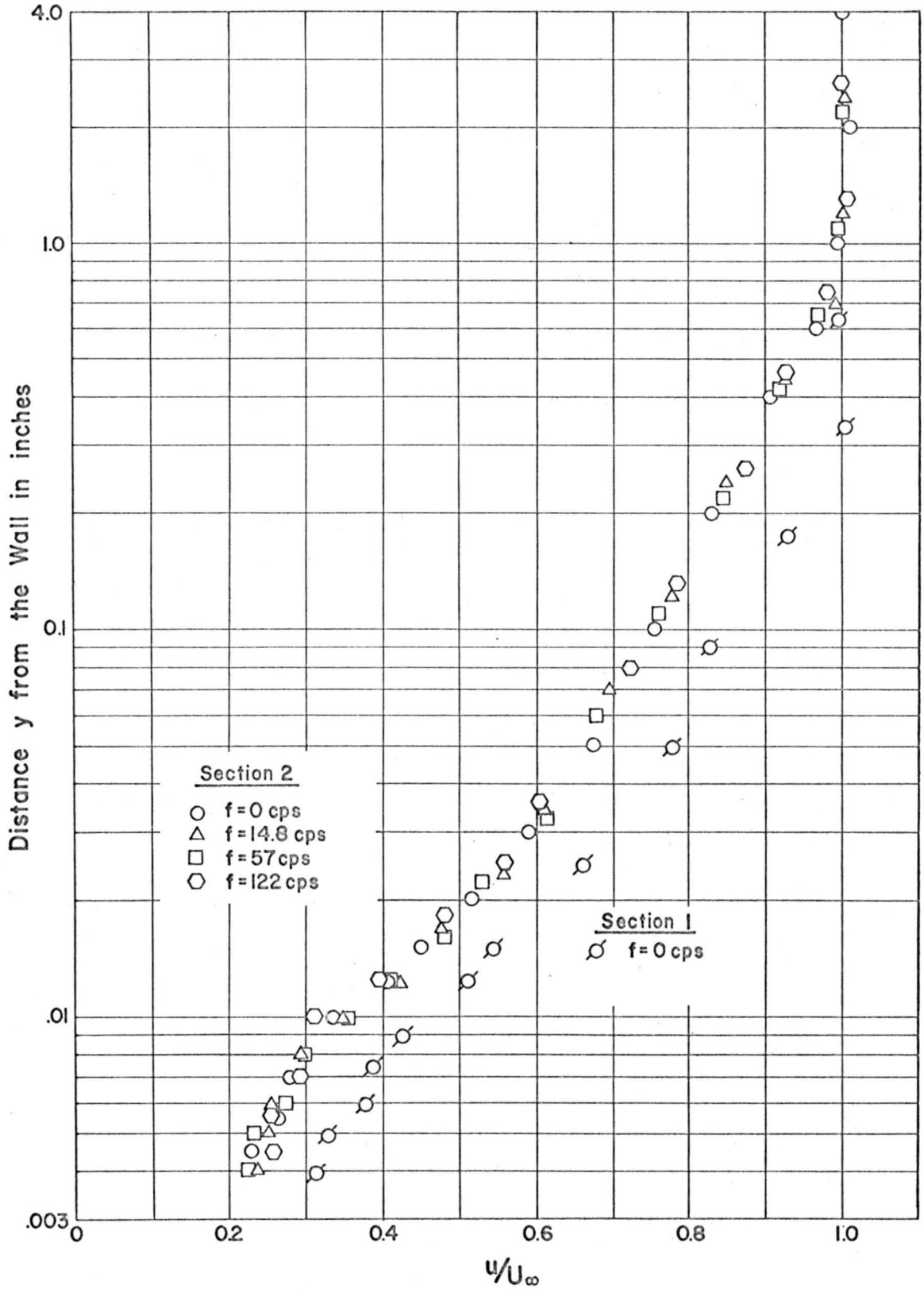

Fig. 10 - Boundary Layer Velocities, U_∞ = 2.4 fps

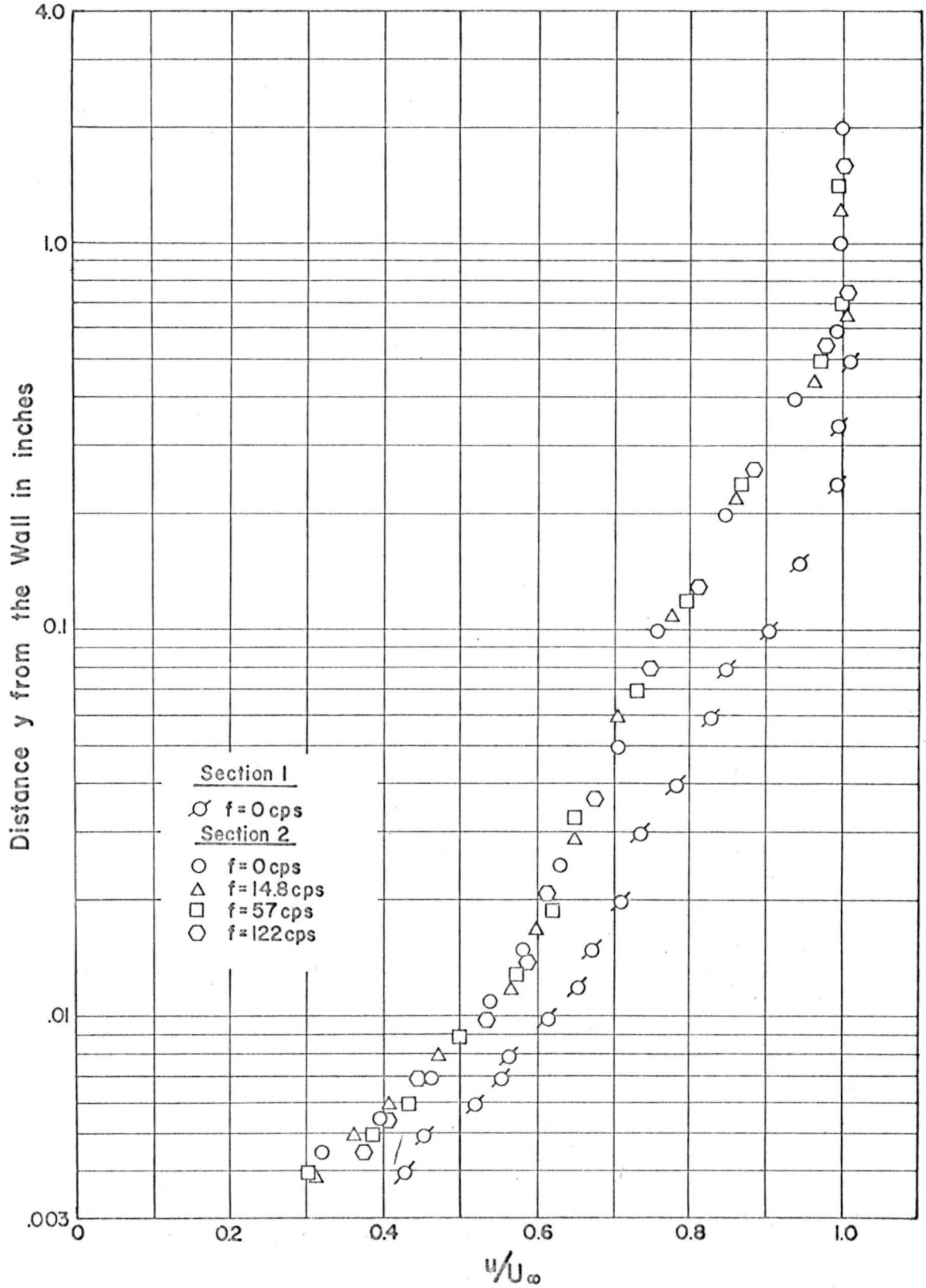

Fig. 11 - Boundary Layer Velocities, $U_\infty = 6.0$ fps

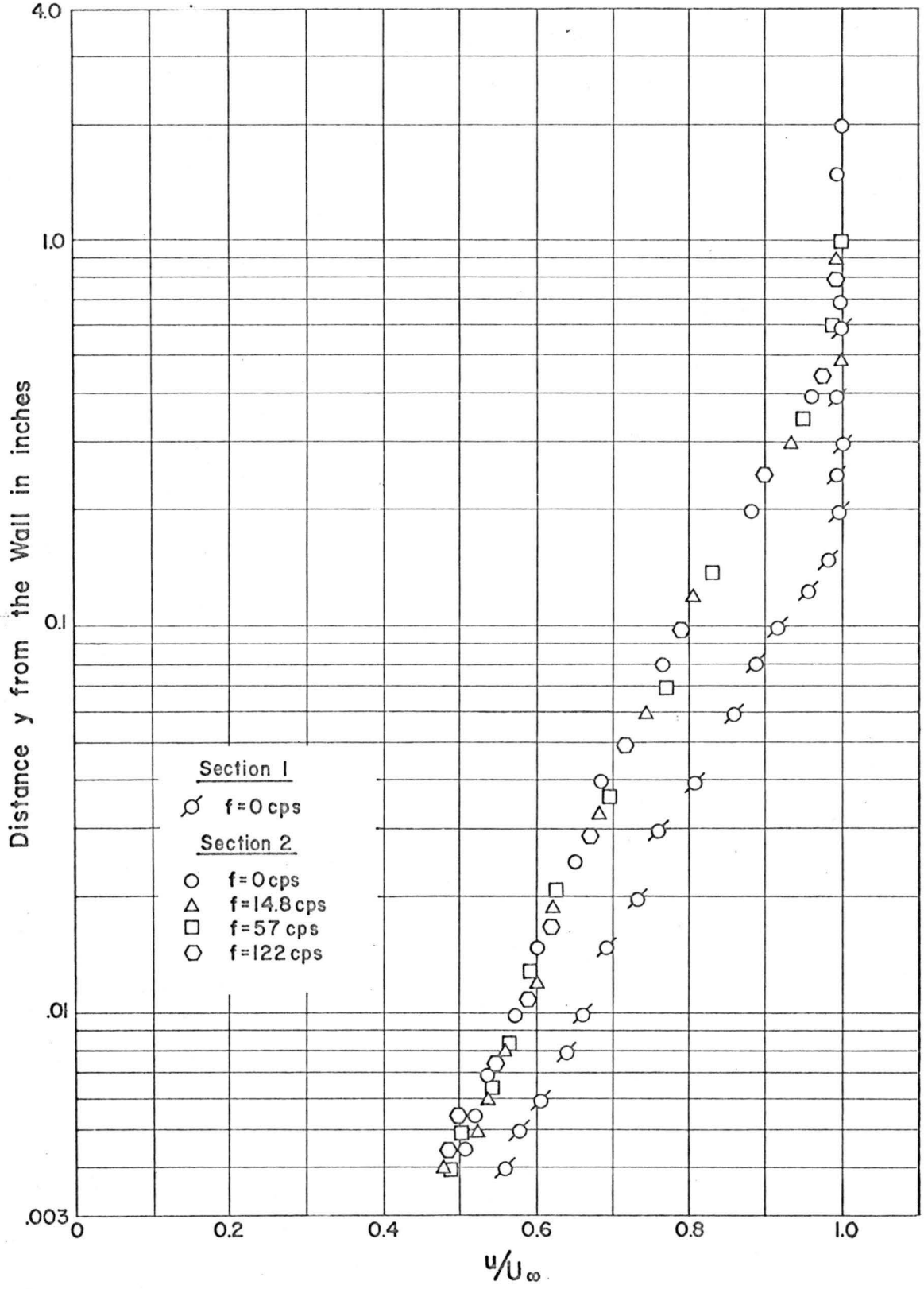

Fig. 12 - Boundary Layer Velocities, U_∞ = 15 fps